Issue
004

Reports on ICON

DOI: 10.5676/DWD_pub/nwv/icon_004
ISSN: 2628-4898

ecRad in ICON
Implementation Overview

Daniel Rieger

November 2019

Deutscher Wetterdienst
Wetter und Klima aus einer Hand

Max-Planck-Institut
für Meteorologie

DOI: 10.5676/DWD_pub/nwv/icon_004
ISSN: 2628-4898

Publisher

Deutscher Wetterdienst
Business Area “Research and Development”
Frankfurter Straße 135
63067 Offenbach
www.dwd.de

Editors

Sebastian Rast, MPI-M
sebastian.rast@mpimet.mpg.de
René Redler, MPI-M
rene.redler@mpimet.mpg.de
Daniel Reinert, DWD,
daniel.reinert@dwd.de
Daniel Rieger, DWD,
daniel.rieger@dwd.de
Florian Prill, DWD,
florian.prill@dwd.de

ecRad in ICON - Details on the Implementation and First Results

Daniel Rieger[(1)], Martin Köhler[(1)], Robin J. Hogan[(2)], Sophia A. K. Schäfer[(1)], Axel Seifert[(1)], Alberto de Lozar[(1)], and Günther Zängl[(1)]

(1) Deutscher Wetterdienst, Offenbach, Germany
(2) ECMWF, Reading, United Kingdom

This document refers to release icon-2.6.0.

Abstract

The new radiation package ecRad from ECMWF (European Centre for Medium-Range Weather Forecasts) has been successfully implemented into the numerical weather prediction (NWP) physics package of ICON. This article describes the concept of the implementation, lists assumptions that have been made and provides an overview on the available namelist settings to control ecRad. First results are presented including a comparison with the RRTM (Rapid Radiative Transfer Model) radiation scheme currently used operationally for NWP and a comparison with CERES (Clouds and the Earth's Radiant Energy System) observational data.

Keywords: radiation, NWP, ecRad

Correspondence to: Daniel Rieger (daniel.rieger@dwd.de)

1. Introduction

The radiation scheme ecRad (Hogan and Bozzo, 2018) offers many potential benefits compared to the currently used RRTM implementation in ICON. In contrast to the current RRTM implementation, the ecRad source code is being actively maintained, well documented (e.g., Hogan, 2018), and new developments are being incorporated into the code. Parameterizations are more consistent than in the currently used RRTM implementation (e.g., in the RRTM implementation the cloud overlap is different for short and long wave). ecRad is coded in a flexible and modular way which enables a wide range of applications. This makes it a perfect addition to the seamless ICON model framework.

There are some differences in the physics as compared to the currently used RRTM implementation. The McICA solver (Monte-Carlo Independent Column Approximation, Pincus et al., 2003) offers a way to account for sub-grid scale inhomogeneities. Two further solvers are available. The Tripleclouds solver (Shonk and Hogan, 2008) accounts for horizontal inhomogeneity of clouds by using three distinct regions in every grid box: optically thicker clouds, optically thinner clouds

and clear sky. SPARTACUS (SPeedy Algorithm for Radiative TrAnsfer through CloUd Sides, Hogan et al., 2016, Schäfer et al., 2016) captures 3-dimensional effects in a two-stream radiation scheme.

The current RRTM implementation in ICON neglects the impact of longwave scattering by clouds and aerosols. For ecRad, longwave scattering can be activated for clouds and aerosols independently. Longwave scattering by clouds but not aerosols is an especially interesting feature, as it is computationally cheap and has the potential to significantly improve the results.

For these reasons, it has been decided to implement and test ecRad in ICON. This manuscript provides an overview on the implementation strategy of ecRad in ICON (section 2) followed by a list of assumptions used for the implementation (section 3). Finally, some first results are shown in section 4. In appendix A, the available ICON namelist options and a valid configuration of ecRad are listed.

2. Implementation Concept

The general idea for implementing ecRad as an option for the radiative transfer scheme is to include it as an external library. With this approach, it is ensured that no dependencies of ecRad from the host model ICON are created. On the ICON side, a module named `mo_ecrad` serves as the adapter between the ICON code and the ecRad code. No other ICON module makes explicit use of ecRad routines or ecRad data structures. This approach ideally also allows us to take a new version of the ecRad code from ECMWF and simply plug it into ICON without any further modification of the ecRad code. However, for the first implementation some issues in the ecRad code had to be fixed. These fixes are expected to be provided with future ecRad releases.

In order to use ecRad, the ICON code has to be configured with an additional flag `--with-ecrad`. This activates a preprocessor makro `#ifdef __ECRAD`. All ICON modules that are directly associated with ecRad (i.e., `mo_ecrad`, `mo_nwp_ecrad_init`, `mo_nwp_ecrad_interface`, `mo_nwp_ecrad_utilities` and `mo_nwp_ecrad_prep_aerosol`) are seen as nearly empty by the compiler otherwise.

The calling tree starting from ICON's NWP physics initialization during the model initialization and from ICON's NWP radiation interface during time stepping down to the ecRad code is depicted in Figure 1.

In the initialization phase of the ICON model, the ecRad initialization inside the module `mo_ecrad_init` is called from `mo_nwp_phy_init`. `mo_ecrad_init` consists of several types of settings. First of all, the precision of real variables in ecRad is taken from a kind value named `jprb` (originating from IFS). This kind value is not necessarily the same as the working precision `wp` used by ICON. Hence, a consistency check between the kind value `wp` from ICON and the ecRad internal kind value `jprb` is performed by comparing `PRECISION` and `EPSILON`. Selected settings are taken from ICON namelist options and then translated into ecRad settings (e.g., choice of the cloud overlap scheme, for more details see Table 2). Parts of the available ecRad configuration options are currently hardcoded. Most notably, ecRad in ICON is currently configured to work

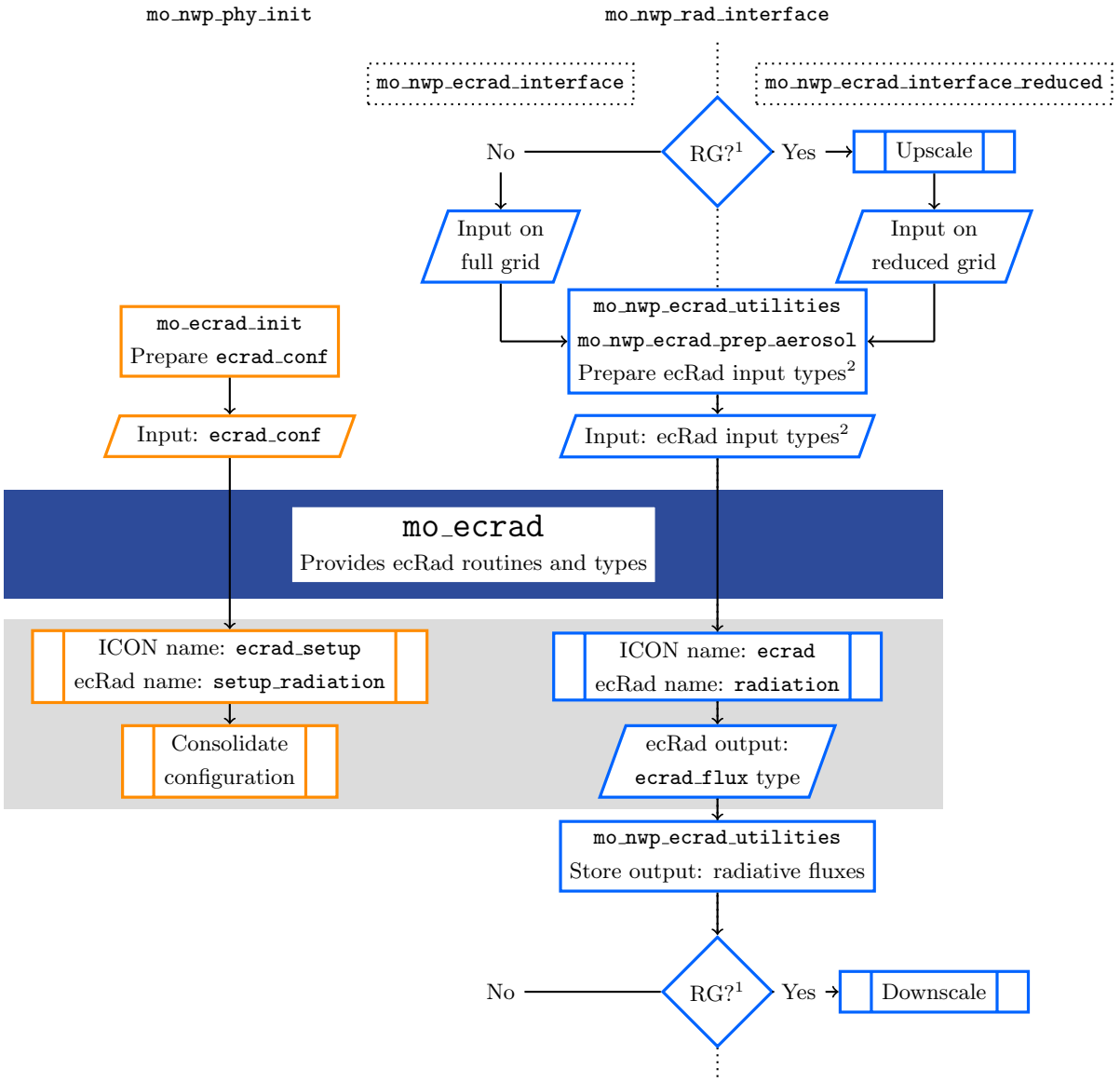

Figure 1: Workflow of the interface between ICON and the ecRad code. The grey shaded parts are code parts executed within ecRad, i.e., the corresponding code can be found inside the directory `externals/ecrad`.
[1]RG stands for reduced grid. This is activated by the namelist parameter `lredgrid_phys` in `grid_nml`.
[2]ecRad input types are: `ecrad_single_level`, `ecrad_thermodynamics`, `ecrad_gas`, `ecrad_cloud` and `ecrad_aerosol`.

only with the McICA solver (Pincus et al., 2003) for the simple reason that other options are not tested to work with ICON. An experienced user may still choose another solver by modifying the code in `mo_ecrad_init`. Finally, settings which are specific for the data used by ICON are transferred to ecRad (e.g., albedo data wavelength intervals).

During the time stepping, the ICON routine `mo_nwp_rad_interface` calls one of the two interface options for ecRad. More specifically, the frequency for radiation calls is given by the user-defined intervall `dt_rad` (namelist `nwp_phy_nml`). Based on the namelist parameter `lredgrid_phys` (namelist `grid_nml`), the radiation is either calculated on the dynamics grid or on the corresponding parent grid which has a factor of 4 fewer horizontal grid points. Depending on this choice, either `nwp_ecrad_radiation` or `nwp_ecrad_radiation_reduced` is called. In the interface for radiation on a reduced horizontal grid, an upscaling of input fields is performed at the beginning and a downscaling of the output fields is performed at the end of the interface. Besides the up- and downscaling, the workflow in the interfaces for radiation on full and reduced grid is similar.

The interfaces to ecRad have to fill several ecRad data structures with input from ICON. These data structures are `ecrad_aerosol`, `ecrad_gas`, `ecrad_cloud`, `ecrad_thermodynamics` and `ecrad_single_level`. Similarly, the output of ecRad, i.e. the radiative fluxes, is stored in a data structure named `ecrad_flux`. Filling these data structures with values from ICON is done independent from the choice of `lredgrid_phys`. Unified subroutines to fill the ecRad aerosol data type are provided by `mo_nwp_ecrad_prep_aerosol`. Unified subroutines to fill the other data types are provided by `mo_nwp_ecrad_utilities`. These unified subroutines ensure consistency between the two interfaces if a data structure is filled with expert knowledge (e.g., calculation of the cloud particle effective radius). Filling the ecRad data structures is done by either copying data from ICON data structures (if available) or by calculation of the data and storage in ecRad data structures.

3. Assumptions

The aim of this section is to describe (currently hardcoded) assumptions that are made during the initialization and on the interface level of the ICON-ecRad coupling. For assumptions that are made within ecRad, please see Hogan and Bozzo (2018).

- As stated in the previous section, the McICA solver (Pincus et al., 2003) is chosen.
- The only available option for the gas optics is currently RRTM.
- The SW delta-Eddington scaling is applied for cloud and aerosol scattering properties before it is merged with gases (`do_sw_delta_scaling_with_gases = .FALSE.`).
- There are different thresholds chosen:
  - A cloud is present if cloud fraction exceeds 10^{-6} (`cloud_fraction_threshold`) and total cloud mixing ratio (ice+water, including subgrid-scale contribution) exceeds $10^{-9}\,\mathrm{kg\,kg^{-1}}$ (`cloud_mixing_ratio_threshold`).
  - For LW, a minimum gas optical depth of 10^{-15} is set for stability reasons (`min_gas_od_lw`). In SW, this value is set to 0 (`min_gas_od_sw`). Note that the RRTM gas optics work with internal thresholds for gas concentrations.

- The fractional standard deviation of in-cloud water content (FSD) is set globally constant to 1.
- The ratio of the overlap decorrelation length for cloud inhomogeneities to the overlap decorrelation length for cloud boundaries is set to 0.5 (`cloud_inhom_decorr_scaling`).
- The cloud particle effective radius calculation has been taken over from a currently used implementation in ICON in the module `mo_newcld_optics`. The equations can be found in Roeckner et al. (2003).

4. First Results

Two sets of daily 24 hour forecasts were conducted for January 2018. The first set named ICON-RRTM serves as a reference, using ICON with the currently operationally used RRTM radiation scheme. The second set termed ICON-ecRad uses ICON in combination with the newly implemented ecRad radiation scheme. In both cases, the generalized overlap assumption (`icld_overlap = 2`) is chosen. ICON-ecRad is using the default cloud properties (`iliquid_scat = 0` and `iice_scat = 0`). Longwave cloud scattering is activated for ICON-ecRad (`llw_cloud_scat = .true.`, not implemented for ICON-RRTM). The settings for trace gas concentrations and aerosol concentrations are identical to the current operational NWP setup (see Table 1).

Table 1: Settings for trace gas concentrations and aerosol concentrations.

Species	Concentration
Aerosol	Tegen aerosol climatology
H_2O	From water vapor tracer of ICON
O_3	GEMS climatology with blending to MACC over Antarctica
CO_2	Globally constant volume mixing ratio $= 390 \cdot 10^{-6}$
CH_4	tanh profile with surface volume mixing ratio $= 1800 \cdot 10^{-9}$
N_2O	tanh profile with surface volume mixing ratio $= 322 \cdot 10^{-9}$
CFC11	Globally constant volume mixing ratio $= 240 \cdot 10^{-12}$
CFC12	Globally constant volume mixing ratio $= 532 \cdot 10^{-12}$

Figure 2 shows comparisons of ICON-ecRad (top row) and ICON-RRTM (bottom row) with Energy Balanced and Filled (EBAF) data from CERES (Clouds and the Earth's Radiant Energy System) (Loeb et al., 2018) for January 2018. The global root mean square error (RMSE) for the net shortwave flux (left column) at the top of the atmosphere (TOA) is reduced from 18.6 $\mathrm{W\,m^{-2}}$ for ICON-RRTM to 17.2 $\mathrm{W\,m^{-2}}$ for ICON-ecRad. This corresponds to a relative change of 7.7 %. Especially in the Intertropical Convergence Zone (ITCZ), ICON-ecRad performs better. There are slight improvements in the stratocumulus regions while there are positive biases of similar magnitudes over the Southern Ocean. It should be kept in mind that differences are due to both errors in the radiation scheme and errors in the cloud fields from ICON. So improvements to the fit to observations can not necessarily be attributed purely to the radiation scheme being better which could be right for the wrong reason.

The right-hand column of Figure 2 shows the difference of the net longwave flux at TOA. It is apparent that red colors, i.e. too little upward flux, too little emission or too much extinction, are dominant for ICON-RRTM (bottom) while blue colors, i.e. too little extinction, are dominant for

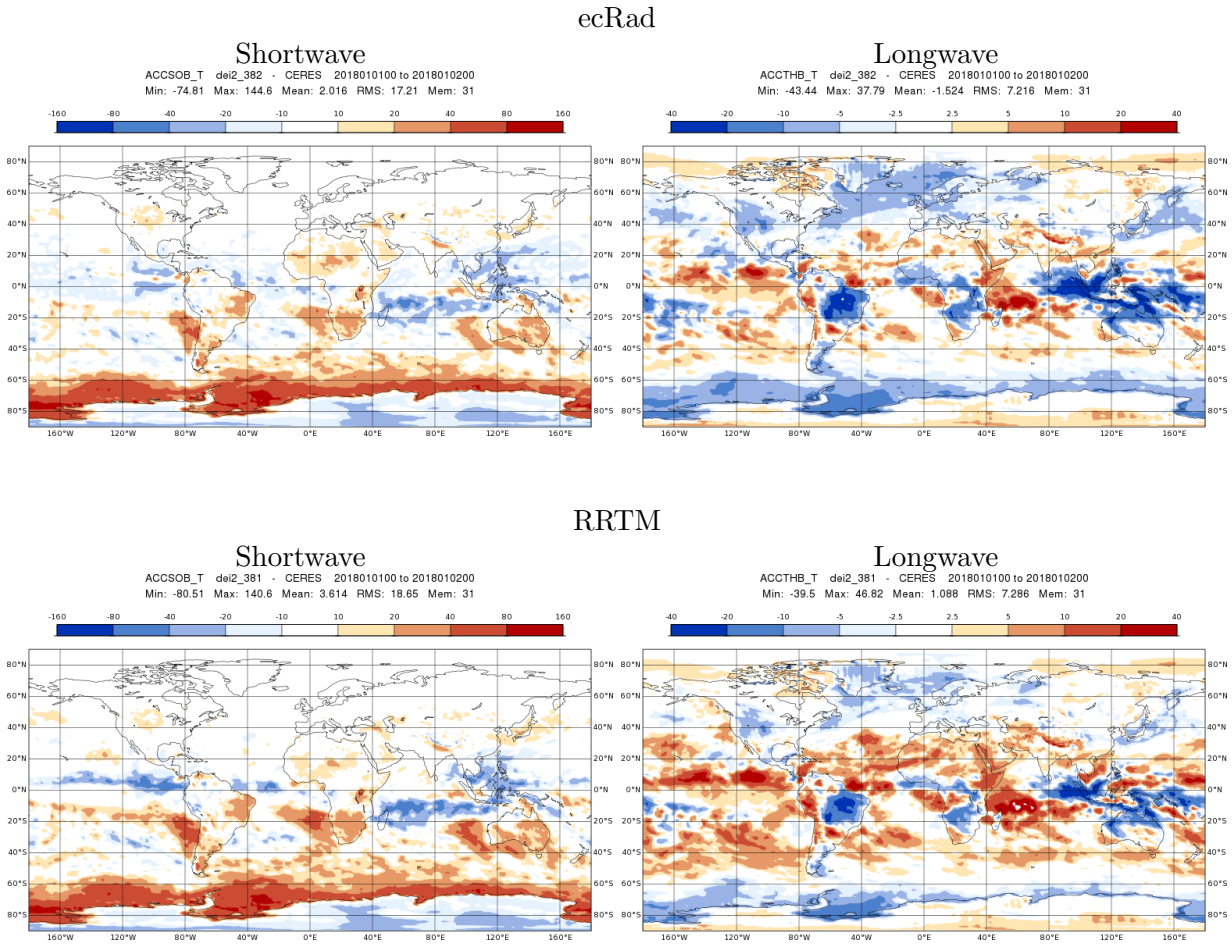

Figure 2: Difference between model output and CERES observational data (Loeb et al., 2018) for one month of daily forecasts for January 2018. Left column: solar net downward flux top of the atmosphere (TOA). Right column: longwave net flux (TOA). Top row: ICON-ecRad, bottom row: ICON-RRTM. Downward fluxes are defined to be positive.

ICON-ecRad. This is reflected by a change in the sign of the bias with $1.1\,\mathrm{W\,m^{-2}}$ for ICON-RRTM and $-1.5\,\mathrm{W\,m^{-2}}$ for ICON-ecRad. The RMSE is slightly reduced from $7.3\,\mathrm{W\,m^{-2}}$ to $7.2\,\mathrm{W\,m^{-2}}$ which corresponds to $\approx 1\,\%$.

The scatter plots in Figure 3 are created with identical global initial data after one integration time step. The purpose is to feed both radiation schemes with the same input and compare the results. The comparison of the shortwave TOA albedo (top left) shows two distinct differences. For low albedo values, ecRad produces slightly higher values ($\approx 2\,\%$) which means that thin clouds are more reflective. For high albedo values, i.e. thick clouds, ecRad is less reflective (also $\approx 2\,\%$).

Figure 3's center left plot visualizes the differences in the TOA longwave net flux. Optically thinner cold, high clouds lead to a difference of $\approx 15\,\mathrm{W\,m^{-2}}$ for ICON-ecRad compared to ICON-RRTM.

Considering only clear sky cases for both, the shortwave albedo (top right) and longwave net

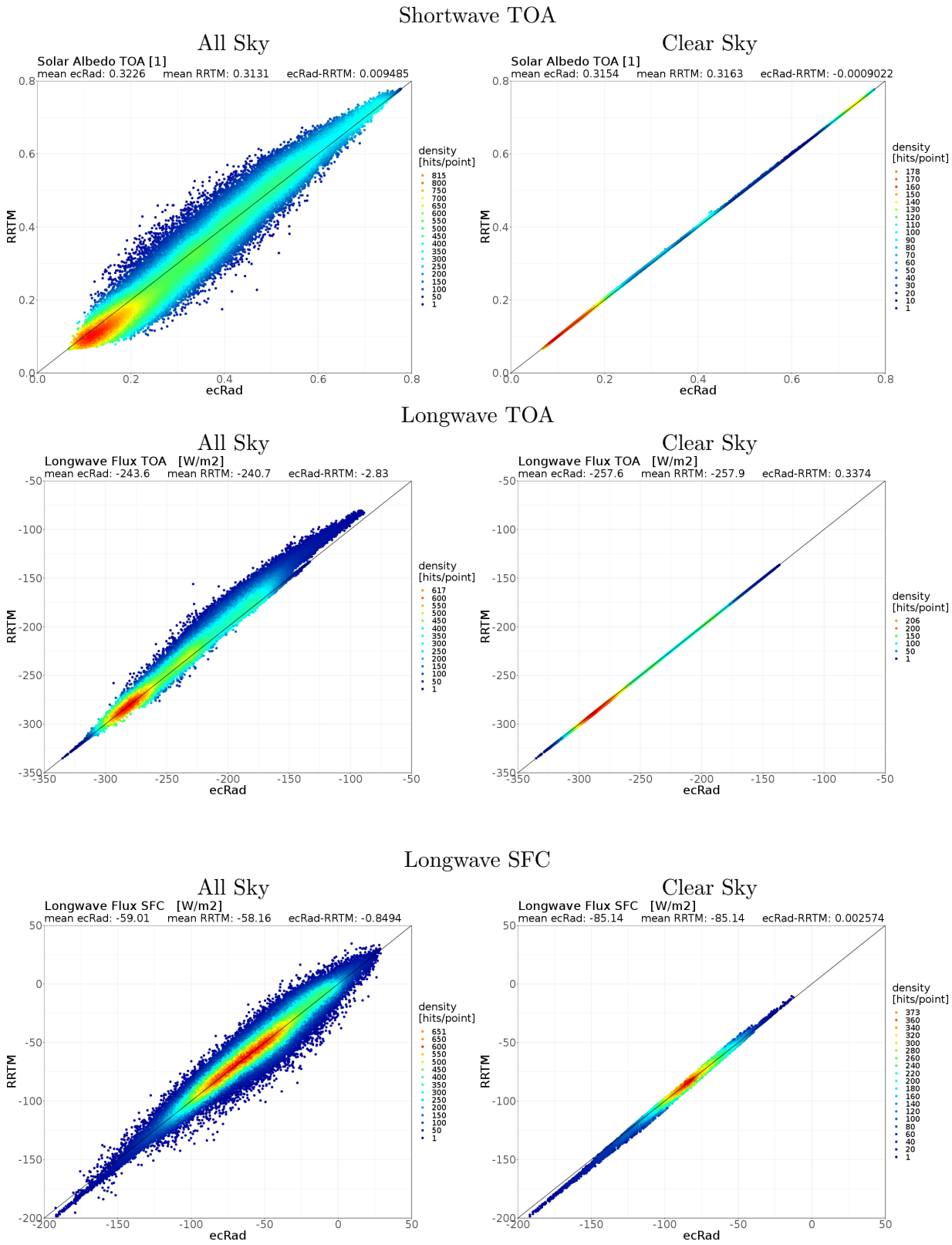

Figure 3: Scatter plots of the differences between ICON-ecRad and ICON-RRTM after one integration time step. Top row: solar albedo at the top of the atmosphere (TOA), all sky (left) and for cloud free grid points (right, total cloud cover $< 1\,\%$). Center row: net longwave flux (TOA) all sky (left) and cloud free (right). Bottom: net longwave flux at the surface all sky (left) and cloud free (right).

flux (center right), the results are nearly identical. This indicates that the major differences between ICON-ecRad and ICON-RRTM are introduced by the treatment of clouds.

The longwave net downward flux at the surface (downward positive) is shown in the bottom left plot of Figure 3. For clear sky columns, there is $\approx 5\,\mathrm{W\,m^{-2}}$ less surface cooling (high negative values). This is caused by an optically thicker clear-sky atmosphere for ecRad. This is confirmed by the same plot for clear sky cases at the bottom right where this systematic difference is visible as well. Low clouds (net longwave flux around $-40\,\mathrm{W\,m^{-2}}$) are optically thinner in ICON-ecRad resulting in a difference of $\approx 5\,\mathrm{W\,m^{-2}}$.

Some of the changes in cloud-radiation interaction could be explained by the two schemes' different cloud geometry parameterizations (overlap, inhomogeneity). Work on understanding these differences and evaluating the two schemes' performance against reality is ongoing.

5. Outlook

Having completed the technical implementation of ecRad in ICON, the focus shifts to a detailed comparison with observations and further parameterization development. To complement satellite observations like CERES we will use surface measurements from the Baseline Surface Radiation Network (BSRN) that provides high quality data from a range of climate regions.

A first focus of further development will be on the optical properties of large ice particles such as snow and graupel. To this end, ecRad will be modified to accept a user-defined number of cloud particle species as input. Further on, work is planned on more detailed descriptions of cloud geometry and the impact of aerosols on radiation.

An important aspect is the computational cost of ecRad compared to the current RRTM implementation. Our preliminary experiences from an ICON-D2 experiment are that the radiation takes about 20 % more runtime using ecRad without longwave scattering by clouds. ICON-D2 is the planned setup for future high-resolution NWP at DWD. Including longwave scattering by clouds it takes about 30 % more runtime than RRTM. This difference might not be representative for global simulations where longwave scattering accounts for $\approx 4\,\%$ in the IFS model (Hogan and Bozzo, 2018). The increase in runtime is not surprising given the improved physics implemented in ecRad especially with respect to the McICA solver. The resulting difference in total runtime for an ICON-D2 setup is less than 1 %. Given the upcoming transition of DWD to a vector architecture, an optimization of the ecRad implementation in ICON will be indispensable.

Acknowledgments

We want to thank Luis Kornblueh, Jan Frederik Engels, Florian Prill and Sergey Kosukhin for their assistance in setting up the configuration environment of ICON for ecRad. We thank Daniel Reinert for reviewing the implementation. The authors acknowledge the usage of CERES EBAF data.

A. Namelist Options

Table 2: Namelist options with a direct interaction with the ecRad configuration. Type I is an integer value, type R a real value and type C a character string.

Parameter	Namelist	Type	Default	Values
inwp_radiation	nwp_phy_nml	I	1	ecRad is activated by inwp_radiation=4
lredgrid_phys	grid_nml	L	.FALSE.	Calculate radiation on a reduced grid?
radiation_grid_filename	grid_nml	C		Grid filename for radiation on coarsest grid. Only needed if lredgrid_phys = .TRUE.
icld_overlap	radiation_nml	I	2	Cloud overlap scheme: 1: maximum random overlap 2: generalized overlap 5: exponential overlap
ecrad_data_path	radiation_nml	C	"."	Path to the folder containing ecRad optical properties files.
llw_cloud_scat	radiation_nml	L	.FALSE.	Long-wave cloud scattering.
iliquid_scat	radiation_nml	I	0	Optical properties used for liquid cloud scattering: 0: SOCRATES 1: Slingo (1989)
iice_scat	radiation_nml	I	0	Optical properties used for ice cloud scattering: 0: Fu et al. (1996) 1: Baran et al. (2016)
irad_aero	radiation_nml	I	2	Aerosols: 0: No aerosol 2: Globally constant 5: Tanre aerosol climatology 6: Tegen aerosol climatology 9: ART aerosol
irad_h2o	radiation_nml	I	1	Water vapor vertical profile: 0: Set to zero 1: Use value from QV tracer

Continued on next page

Table 2: *Continued from previous page*

irad_co2	radiation_nml	I	2	Carbon dioxide vertical profile: 0: Set to zero 2: Constant (vmr_co2)
vmr_co2	radiation_nml	R	348.e-6	CO_2 volume mixing ratio
irad_ch4	radiation_nml	I	3	Methane vertical profile: 0: Set to zero 2: Constant (vmr_ch4) 3: tanh profile (at surface: vmr_ch4)
vmr_ch4	radiation_nml	R	165.e-8	CH_4 volume mixing ratio
irad_n2o	radiation_nml	I	3	Nitrous oxide vertical profile: 0: Set to zero 2: Constant (vmr_n2o) 3: tanh profile (at surface: vmr_n2o)
vmr_n2o	radiation_nml	R	306.e-9	N_2O volume mixing ratio
irad_o3	radiation_nml	I	0	Ozone vertical profile: 0: Set to zero 7: GEMS climatology 9: MACC climatology 79: Blending of 7 and 9 97: Blending of 7 and 9
irad_o2	radiation_nml	I	2	Oxygen vertical profile 0: Set to zero 2: Constant (vmr_o2)
vmr_o2	radiation_nml	R	0.20946	O_2 volume mixing ratio
irad_cfc11	radiation_nml	I	2	CFC11 vertical profile: 0: Set to zero 2: Constant (vmr_cfc11)
vmr_cfc11	radiation_nml	R	214.5e-12	CFC11 volume mixing ratio
irad_cfc12	radiation_nml	I	2	CFC12 vertical profile: 0: Set to zero 2: Constant (vmr_cfc12)
vmr_cfc12	radiation_nml	R	371.1e-12	CFC12 volume mixing ratio

References

Hogan, R. J., 2018: *ecRad radiation scheme: User Guide (draft)*. https://confluence.ecmwf.int/display/ECRAD.

Hogan, R. J. and A. Bozzo, 2018: A flexible and efficient radiation scheme for the ECMWF model. *J. Adv. Model Earth Sy.*, **10**(8), 1990–2008.

Hogan, R. J., S. A. K. Schäfer, C. Klinger, J. C. Chiu, and B. Mayer, 2016: Representing 3-D cloud radiation effects in two-stream schemes: 2. Matrix formulation and broadband evaluation. *J. Geophys. Res.: Atmos.*, **121**(14), 8583–8599.

Loeb, N. G., D. R. Doelling, H. Wang, W. Su, C. Nguyen, J. G. Corbett, L. Liang, C. Mitrescu, F. G. Rose, and S. Kato, 2018: Clouds and the earths radiant energy system (CERES) energy balanced and filled (EBAF) top-of-atmosphere (TOA) edition-4.0 data product. *J. Clim.*, **31**(2), 895–918.

Pincus, R., H. W. Barker, and J.-J. Morcrette, 2003: A fast, flexible, approximate technique for computing radiative transfer in inhomogeneous cloud fields. *J. Geophys. Res.: Atmos.*, **108**(D13).

Roeckner, E., G. Bäuml, L. Bonaventura, R. Brokopf, M. Esch, M. Giorgetta, S. Hagemann, I. Kirchner, L. Kornblueh, E. Manzini, et al., 2003: The atmospheric general circulation model ECHAM 5. PART I: Model description. Technical Report 349, Max Planck Institute for Meteorology.

Schäfer, S. A. K., R. J. Hogan, C. Klinger, J. C. Chiu, and B. Mayer, 2016: Representing 3-D cloud radiation effects in two-stream schemes: 1. Longwave considerations and effective cloud edge length. *J. Geophys. Res.: Atmos.*, **121**(14), 8567–8582.

Shonk, J. K. and R. J. Hogan, 2008: Tripleclouds: An efficient method for representing horizontal cloud inhomogeneity in 1D radiation schemes by using three regions at each height. *J. Clim.*, **21**(11), 2352–2370.